Heliyon 10 (2024) e29277

Contents lists available at ScienceDirect

Heliyon

journal homepage: www.cell.com/heliyon

Research article

Dual Brønsted acidic-basic function immobilized on the 3D mesoporous polycalix [4]resorcinarene: As a highly recyclable catalyst for the synthesis of spiro acenaphthylene/ indene heterocycles

Aref Mahmoudi Asl, Bahador Karami *, Mahnaz Farahi, Zahra Karimi

Department of Chemistry, Yasouj University, P. O. Box 353, Yasouj, 75918-74831, Iran

ARTICLE INFO

Keywords:
Mesopore
Cavity
Host-guest
Porosity
Polymeric catalyst

ABSTRACT

In this study, a novel dual Brønsted acidic-basic nano-scale porous organic polymer catalyst, PC4RA@SiPr-Pip-BuSO3H, was synthesized through various steps: preparation of a 3D network of polycalix, modification with (3-chloropropyl)-trimethoxysilane, then functionalization of polymer with piperazine and *n*-butyl sulfonic acid under the provided conditions. The catalyst characterization was performed by FT-IR, TGA, EDS, elemental mapping, PXRD, TEM, and FE-SEM analyses, confirming high chemical stability, activity, recoverability, and excellent covalent anchoring of functional groups. So, the designed catalyst was utilized for preparing spiro-acenaphthylene and amino-spiroindene heterocycles, providing good performance with a high yield of the corresponding products. Accordingly, this catalyst can be used in different organic transformations. Necessary experiments were conducted for the recyclability test of the polymeric catalyst, and the results showed the PC4RA@SiPr-Pip-BuSO3H catalyst can be reused 10 times without any decrease in its activity or quality with excellent stability. The structure of resultant spiro heterocycles was confirmed using 1H NMR, 13C NMR, and FT-IR.

1. Introduction

One important category of polymer networks is porous organic polymers (POPs). They are made by linking organic monomers together through covalent bonds [1,2]. Their utilization in various fields such as heterogeneous catalysis [3,4], photocatalysis [5,6], separation [7,8], sensing, energy-related applications [9], and adsorption [10] is due to their unique features, including low density, high surface area (>6000 m^2/g), good designability, high thermal stability, tunable porosity, stable physical and chemical properties, and abundance of active sites [11–22]. The POPs divide into two categories: amorphous and crystalline [6,16,17,19,23,24]. These categories themselves consist of two groups with mesoporous and microporous structures [25]. Unlike amorphous pops with flexible and uncomplicated scaffolds that usually require easy synthetic conditions and simple production methods, crystalline covalent organic frameworks (COFs) require specific organic reactions to form their regular porous structures [12,26].

Exclusively microporous polymeric catalysts might hinder the diffusion of reactants due to their small pore size. A possible solution to this problem is using meso/macroporous hierarchical networks [27–29]. POPs have been composed of chemical elements such as C,

* Corresponding author.
E-mail address: karami@yu.ac.ir (B. Karami).

https://doi.org/10.1016/j.heliyon.2024.e29277
Received 21 January 2024; Received in revised form 13 March 2024; Accepted 3 April 2024
Available online 4 April 2024

H, O, N, etc [25]. Usually, a two- or three-dimensional network must be formed to create a polymer with permanent porosity and vacant space. This purpose is achievable if one of the monomers has two or more functional groups. Porosity facilitates the penetration of organic materials into the active sites of catalysts. Therefore, it seems that only a few polymers, such as inherently porous polymers, have porosity, while most linear polymers lack pores [30–35]. Improved accessibility to catalytic properties is possible due to the easy modification of POPs (post-synthesis modification) before and after synthesis. As a result, they are suitable solid supports for the production of heterogeneous catalysts [36–41].

Calixarenes, produced through the reaction between phenols and aldehydes, are classified as macrocyclic compounds. They have empty spaces that introduce them as new hosts for use in supramolecular chemistry [42–48]. In supramolecular chemistry, these pores are used as absorption and retention sites of small and large molecules, which is beneficial for forming complex and novel structures. Calixarenes can interact with guest molecules through electrostatic interactions and non-covalent forces such as hydrogen bonding [49,50]. Calixarene modification was achieved through stable covalent bonding and resulted in a macrocycle with high thermal stability and hardness. This modification can create a well-organized network of porosity and allow for greater accessibility to functional groups, which are responsible for confinement or attachment to the analyte [51,52]. Modified calixarenes cause various interactions with diverse guest molecules due to their structural shape. The most stable conformation of *Cis*-calix [4]a renes (C4A) is cup-like with the lowest energy [53]. Modified calixarenes can be used for diverse applications such as ionophores, alkali metal-complexing agents, heavy metal chelators, and chemical sensors [54,55]. Also, their aromatic nature and insolubility in water make them suitable as phase transfer catalysts [43].

Calix [4]resorcinarene (C4RA) is one of the derivatives of C4A, made up of four resorcinol units connected by methylene bridges [56,57]. The substituent groups at the methylene bridges determine the conformers of C4RA, resulting in five stable isomers [56, 58–62]. Modifying C4RA through various functional groups onto the eight hydroxyphenyl groups and aromatic rings provides a versatile platform for their multi-purpose use. The porosity resulting from the presence of hydrophilic and hydrophobic layers in their structure creates unique characteristics, paving the way for further development and transformation into three-dimensional network polymers [63–65]. In recent years, reports have been published on a new generation of porous organic polymers that exhibit exceptional properties so that these properties are not readily available in other porous materials [66,67]. The use of C4RA as versatile host molecules has attracted attention in various fields, including materials science [68–70], supramolecular chemistry [71,72], and life sciences [73–75].

Piperazine (1,4-diazacyclohexane) is one of the most well-known organic bases with high catalytic activity for preparing organic heterocycles. However, separating piperazine from a homogeneous crud mixture is difficult since neutralization must be performed under acidic conditions, leading to useless ammonium salts. Stabilizing piperazine on a solid support (silica, polymer, etc.) to create a heterogeneous catalyst is the preferred method to remove the destructive effects of acidic workup [76–79].

The immobilization of sulfonic acid in the solid supports is a viable option for taking advantage of the unique properties of heterogeneous catalysts, such as easy separation, high selectivity, and good activity. On the other hand, by immobilizing *n*-butyl sulfonic acid onto solid supports, it is possible to utilize sulfonic acid as mobile active sites for the catalytic system. Additionally, this approach allows us to benefit from flexibility and mobility similar to homogeneous catalysts. The ring-opening of 1,4-Butane-sultone is a common way to produce mobile arms of *n*-butyl-SO_3H connected to the supports [80–84].

Recently, there has been significant progress in developing spiro compounds for creating highly active pharmaceutical molecules. These compounds, with their complex and inflexible three-dimensional structures, exhibit unique biological and pharmacological activities. Spiro compounds, such as spiroacenaphthylene and amino-spiroindene heterocycles, belong to the 4*H*-pyran family and are found in many bioactive natural alkaloids [85,86]. These compounds have been introduced as anti-HIV, anti-tuberculosis, antifungal, anticonvulsant, anticancer, MDM2 inhibitors, and progesterone receptor modulators. They also show outstanding activity as anti-hypertensive agents and have gained attention as new analgesic agents [87–91]. Also, the 4*H*-pyran products bearing a –CN functional group are worthy intermediates in the synthesis of a broad spectrum of compounds, e.g., amino pyrimidines, lactones, pyranopyrazoles, pyridones, 1,4-dihydropyridines, and imido esters [92–97].

More recently, different heterogeneous catalysts such as Fe_3O_4@SiO_2/ECH/IG (based on collagen protein) [98], Fe_3O_4@CS-SO_3H NPs, Bmim(OH)/chitosan/C_2H_5OH (based on chitosan) [99,100], PANI/Fe_3O_4/CNT (based on polyaniline) [101], helical polymer (single-handed helical polyisocyanides) [102], nano-cellulose-$SbCl_5$ [103], Cu_2O@MCC (based on cellulose) [104], PS@GO-Fe_3O_4 (based on polystyrene) [105], PEG-Ni NPs and PEG-OSO_3H (based on polyethyleneglycols) [106,107] have reported for the synthesis of various spiro-compounds.

As a part of our previous research on heterogeneous polymeric support, current work has presented a bifunctional Brønsted acidic-basic catalyst composed of a hybrid of *n*-butyl sulfonic acid and piperazine, stabilized on a cavity-containing polymer based on C4RA. PC4RA@SiPr-Pip-BuSO_3H catalyst was synthesized, characterized, and used in preparing spiro-acenaphthylene and amino-spiroindene heterocycles, which showed satisfactory catalytic performance. These results confirmed the high power of catalyst activity in organic transformations to be further employed.

2. Experimental

2.1. General information

Materials from Merck, Fluka, and Aldric companies were available in all steps. The Japanese instrument (Rigaku Ultima IV) recorded X-ray powder diffraction (PXRD) analysis. Particle placement and morphology were determined using the Philips transmission electron microscope (TEM) and the field emission scanning electron microscope (FE-SEM) using SIGMA VP apparatus from

Zeiss Company of Germany. The FT-IR spectrum was recorded and presented on KBr disks using the JASCO FT-IR/680 plus Fourier transform infrared spectrometer. The electrothermal device (KSB1N) was employed to determine the melting point of synthesized compounds and compare them with previous reports. Reaction progress was controlled by using SIL G/UV254 TLC plates. The Thermal Gravimetric Analysis (TGA) device was applied to evaluate the thermal stability using PerkinElmer STA6000 manufactured by the United States. ^{1}HNMR and ^{13}CNMR analyses were taken by a Bruker Avance instrument, 300 and 75 MHz, respectively. TMS and DMSO-d_6 were applied as an internal standard and the solvent in all spectra, respectively.

2.2. The prepration of Cis-calix [4]resorcinarene (I)

At first, the monomer, namely *Cis*-calix [4]resorcinarene, was acquired through a condensation reaction between acetaldehyde (4 mmol, 0.18 g) and resorcinol (4 mmol, 0.44 g) in the presence of H_2O:EtOH:HCl with the ratio of 2:2:1 (10:10:5 mL) at room temperature under constant stirring for seven days. The reaction progress was monitored by using TLC. After completing the reaction and appearing white crystals, the raw mixture was filtered and washed during the tree sequences stage with cold H_2O and H_2O/EtOH (1:1). Then, the obtained solid was recrystallized from hot EtOH to get a pure product, leading to the *Cis*-C4RA. Our previous reports have confirmed the accuracy of this synthesis through FT-IR, ^{13}C NMR, ^{1}H NMR, and PXRD analyses [95,108].

2.3. The synthesis of polycalix [4]resorcinarene (II)

To prepare polycalix [4]resorcinarene, 21 mmol (11.20 g) of produced *Cis*-calix [4]resorcinarene in the first stage was mixed with 55 mL of aqueous NaOH solution (10%). Initially, while maintaining the reaction at room temperature, 63 mmol (1.89 g) of formaldehyde was slowly and uniformly added to the above mixture. Then, the temperature gradually increased to 90 °C (24 h). The excess alkali was deleted with distilled H_2O, and the remaining was kept in an oven at 95 °C for 1 h. Stirring the obtained solid in the solution of 0.1 M HCl generated the acidic form. Finally, the obtained brown-colored material was dried at 90 °C in the oven for an appropriate

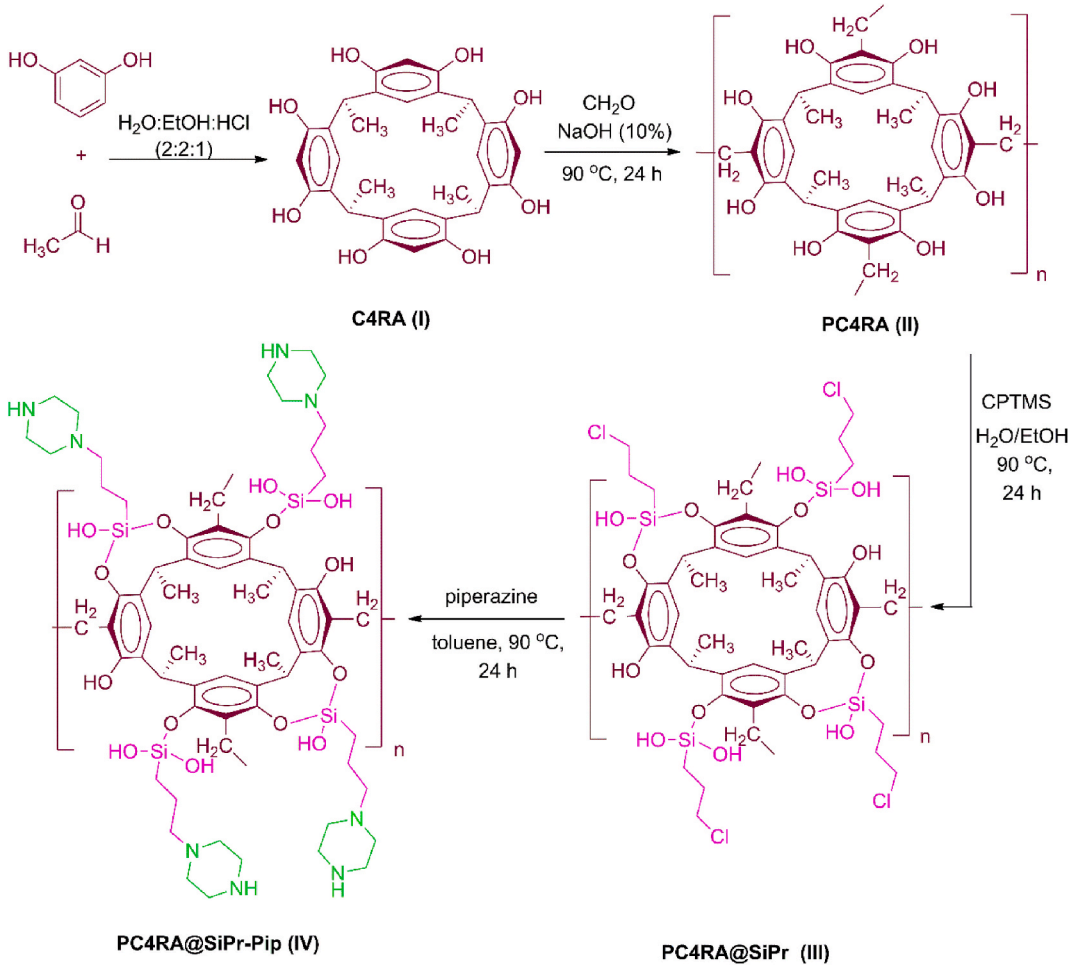

Scheme 1. An outline of the step-by-step synthesis of PC4RA@SiPr-Pip (IV).

time [95,108].

2.4. 2.4synthesis of PC4RA-SiPrCl (III)

The formed polycalix (0.75 g) was placed in a round bottom flask at ambient temperature. The flask contained dissolved (3-chloropropyl)-trimethoxysilane (CPTMS, 12 mmol equal to 2.4 g) in 15 mL of solvent (H_2O/EtOH, 1:1). The obtained mixture was then warmed to 90 °C and stirred for 24 h. After, PC4RA-SiPrCl was extracted and consecutively washed with H_2O/EtOH. It was kept at

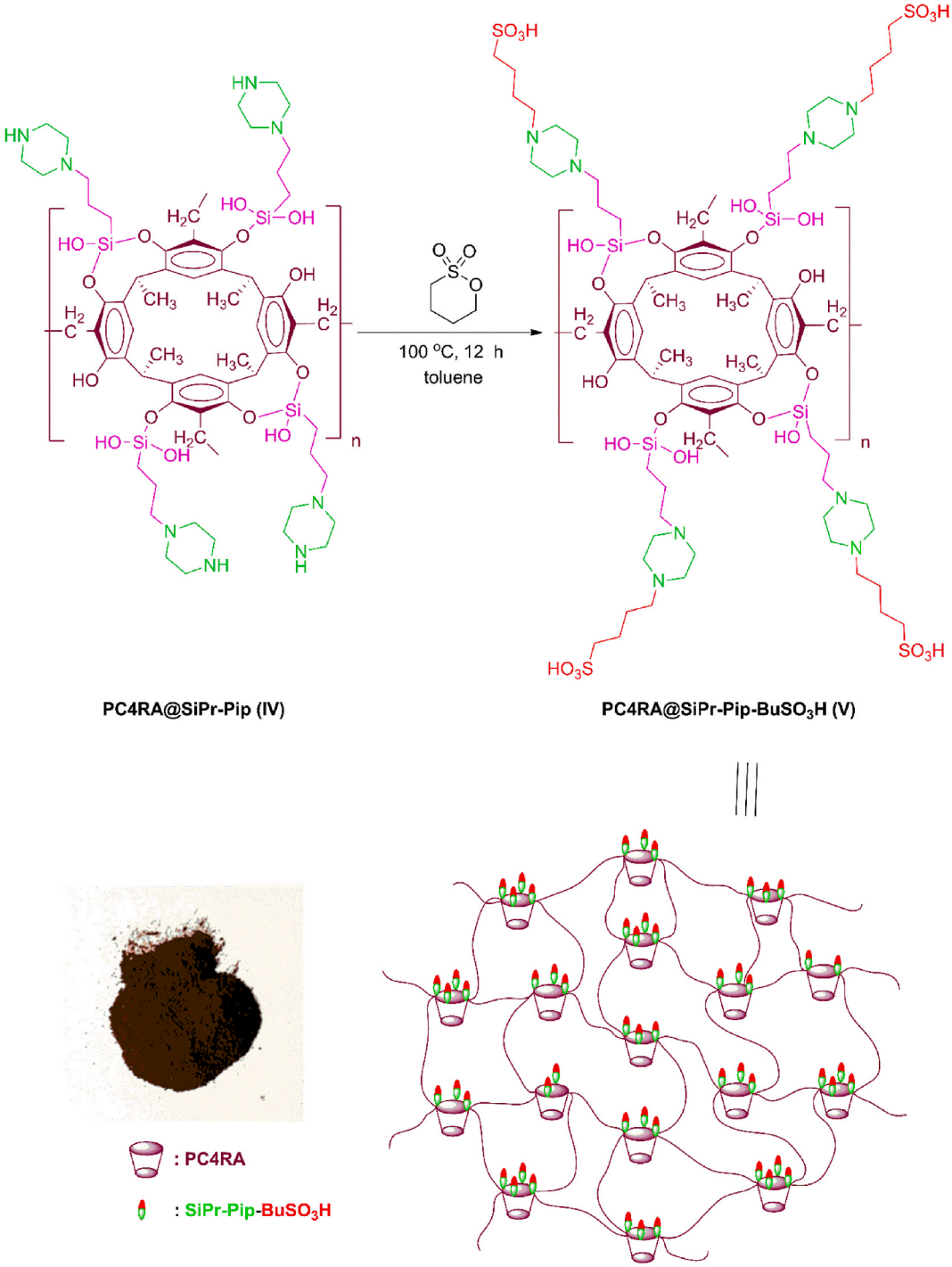

Scheme 2. An outline of final step of PC4RA@SiPr-Pip-BuSO_3H synthesis.

90 °C for 6 h to dry.

2.5. Synthesis of PC4RA-SiPr-Pip (IV)

In this stage, for preparation of the functionalized polymer, piperazine (24 mmol, 2.06 g) and PCRA@SiPrCl (0.75 g) were added to 20 mL of dehydrated toluene into a balloon and stirred for 24 h at a temperature of 90 °C. PC4R@SiPr-Pip was extracted from the reaction mixture and washed several times with the H_2O/EtOH mixture. Finally, it was dried using an oven at 90 °C for 4 h.

2.6. Synthesis PC4RA@SiPr-Pip-BuSO$_3$H (V)

In the final stage of the preparation of PC4RA@SiPr-Pip-BuSO$_3$H, PC4RA@SiPr-Pip and 1,4-butane sultone with an equal ratio of 5.5 mmol (0.75 g) were added into a balloon containing 25 mL of anhydrous toluene. The delivered mixture was stirred at 100 °C for 12 h. The acquired catalyst was separated using a filter and rinsed with ethanol and diethyl ether. Finally, the obtained solid was collected and dried for 4 h at 90 °C in an oven. Synthetic processes of PC4RA@SiPr-Pip-BuSO$_3$H are depicted by Schemes 1 and 2.

2.7. A general method for the synthesis of spiro-acenaphthylene heterocycles

Malononitrile (1 mmol, 0.06 g), acenaphthoquinone (1 mmol, 0.18 g), beta-carbonyls (1 mmol), and catalyst PC4RA@SiPr-Pip-BuSO$_3$H (0.009 g) were mixed by stirring inside a flask containing water (10 mL). The obtained mixture was warmed and left to reflux at 50 °C, followed by TLC monitoring. After 10 min, while completing the reaction, hot EtOH/EtOAc (1:1) was added to the raw mixture to solve the materials. Then, it was immediately filtered so that the catalyst remained over the filter and the crude mixture under the filter. After removing the solvent, the resultant product was washed with H_2O at the first stage and then with a mixture of H_2O/EtOH. The product was recrystallized from hot ethanol and dried at 100 °C for 6 h. The formation of spiro derivatives was confirmed using FT-IR, ^{1}HNMR, ^{13}CNMR spectroscopy, and melting point (See ESI).

3. Results and discussion

3.1. Characterization of catalyst

In the context of designing a material that can be useful in catalytic and non-catalytic areas (such as capacitors and sensors) and enhance the practical application of polycalix [4]resorcinarene, we decided to synthesize, identify, and evaluate newly functionalized polycalix [4]resorcinarene as a bifunctional acidic-basic cavity-containing polymer in the synthesis of spiro-acenaphthylene and amino-spiroindene heterocycles. The prepared bifunctional polymeric catalyst, PC4RA@SiPr-Pip-BuSO$_3$H, was characterized using FT-IR, EDX, TGA, FE-SEM, Elemental mapping, PXRD, and TEM analyses.

The FT-IR spectroscopy exhibited functional groups of the bare PC4RA and modification of the polymer surface at different stages (Fig. 1). In all IR spectra from uncoated PC4RA to functionalized PC4RA, the broad signal around 3280-3550 cm^{-1} is related to the vibration of the OH group of the polymer (Fig. 1a–d). Two distinctive vibration bands at 1107 and 895 cm^{-1} are attributed to the Si–O stretching modes of CPTMS, showing successful silylation of PC4RA (Fig. 1b).

Identical peaks witnessed at the same regions of 2950–3100 cm^{-1} are related to the symmetric stretching vibration of C–H bands for PC4RA, PC4RA@SiPrCl, PC4RA@SiPr-Pip, and PC4RA@SiPr-Pip-BuSO$_3$H (Fig. 1a–d). Also, the NH group shows the absorption band overlapped with the OH group of the polymer (Fig. 1c). The occurred absorption peak at 1128 cm^{-1} is related to the S═O stretching vibrations, successfully confirming the covalent connection of n-BuSO$_3$H on the polymer surface. In addition, due to the overlapping of the OH peak of SO$_3$H with OH of polycalix, they emerge in the same region (Fig. 1d). According to the resultant data, FT-IR analyses demonstrate that Bu-SO$_3$H as a Brønsted acid active site and piperazine have well anchored on the surface of PC4RA

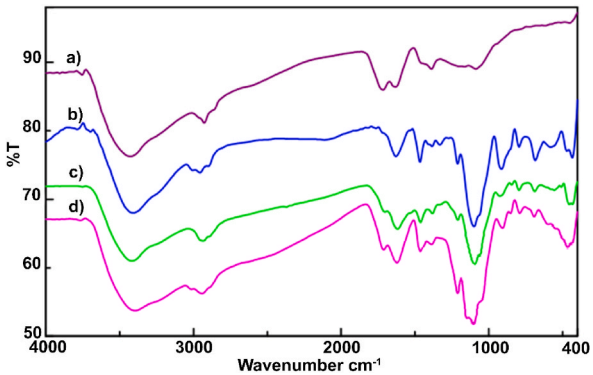

Fig. 1. FT-IR spectrum (KBr pellet, sample: KBr 1:8) of PC4RA (a), PC4RA-SiPrCl (b), PC4RA-SiPr-Pip (c), PC4RA@SiPr-Pip-BuSO$_3$H (d).

support.

The EDX (Energy-dispersive X-ray) technique was studied in the context of approving the

chemical composition of the PC4RA@SiPr-Pip-BuSO$_3$H catalyst (Fig. 2). This pattern well indicated that the desired elements (namely, C, Si, O, S, and N) were present in the polymeric structure in excellent proportions and the starting materials were successfully attached to the polymeric support.

In addition, the elemental mapping analysis was conducted to show elemental composition and the homogeneous distribution of expected elements (Fig. 3). The uniform distribution and good immobilization of functional groups throughout the polymeric support excellently approved the FT-IR and EDX findings.

The structural feature of PC4RA@SiPr-Pip-BuSO$_3$H was analyzed using the WPXRD (wide-angle powder X-ray diffraction) technique (Fig. 4). The observed bread peak around $2\theta \approx 16\text{-}23^{o}$ in the XRD patterns of catalyst indicated that the catalyst had an amorphous structure. This analysis also demonstrated that the amorph nature of the polymer remained intact after adding the acidic functional groups.

As shown in Fig. 5, the low-angle powder X-ray diffraction (LPXRD) of the designed polymer, PC4RA@SiPr-Pip-BuSO$_3$H, exhibits a strong signal at $2\theta \approx 0.5^{o}$. Since the appearance of a reflection peak at $2\theta = 0\text{–}10^{\circ}$ suggests the mesopore structure, the desired PC4RA, bearing SiPr-Pip-BuSO$_3$H, is mesopore.

The surface morphology and particle size were determined using FE-SEM images (Fig. 6). These images clearly show that nano-size particles (<35 nm) have settled on the amorphous surface of the polymer. As seen, spherical particles with uniform size have covered the amorphous structure.

Also, the presence of the acidic-basic functions, SiPr-Pip-BuSO$_3$H group, on the surface of polycalix [4]resorsinarene was severely approved using the TEM analysis. As revealed, it is straightforward to identify between the nanoparticles and PC4RA support due to their different morphologies. The TEM image confirms SEM analysis in detail (Fig. 7).

The investigation of thermal stability was studied using the TGA technique (Fig. 8). Generally, three weight losses have appeared between 90 and 600 °C. As it is apparent in the TG curve, a little weight loss below 100 °C is attributed to water removal, remaining in the porosity of the polymer scaffold, which is a regular occurrence. Two sharp decompositions.

At 340 and 500 °C are related to the decomposition of the organic-inorganic hybrid and the organo-silane agent. In other words, 85% of weight loss observed at around 340–600 °C is associated with removing the organic group. Therefore, the TG curve reveals the high thermal stability of the functionalized polymer since the first cleavage appeared at about 340 °C. TG analysis fully confirms the stabilization of functional groups on the polymer surface and verifies FT-IR, EDS, and elemental mapping results.

After the characterization of the catalyst structure, the catalytic performance was evaluated using the green synthesis of spiro-acenaphthylene and amino-spiroindene heterocycles. At the beginning of the spiro synthesis, malononitrile, acenaphthoquinone, and barbituric acid were chosen as model reaction substrates. Then, the pattern reaction was investigated in several solvents (polar and non-polar) and solvent-free situations to determine the optimal conditions, including temperature and catalyst loading (Table 1). According to the investigations, the PC4RA@SiPr-Pip-BuSO$_3$H catalyst showed exceptional performance and the highest yield in water as a green, abundant, non-toxic, and environmentally friendly solvent. (Table 1, entries 1–7). Another study was conducted on the effect of catalyst loading and the absence of the polymeric catalyst on the model reaction. The outputs delivered that 0.009 g of PC4RA@SiPr-Pip-BuSO$_3$H is the most suitable amount and can lead to the highest efficiency. Increasing the amount of bifunctional polymer did not have any effect on improving efficiency and performance (Table 1, entries 7–11). After determining the optimal solvent and catalyst amount, the reaction was monitored at varying temperatures to identify the most effective temperature. As observed, the activation energy required for the model reaction was achievable at 50 °C. Deviating from this temperature reduced reaction efficiency (Table 1, entries 12–15).

Concerning the concluded outputs, H_2O as a green solvent, 0.009 g of catalyst, and 50 °C were picked as optimal conditions, bolded in Table 1 (entry 7). Finally, to demonstrate the SO_3H as the Brønsted acidic active mobile centers of the bi-functional Brønsted acidic-basic catalyst, the pattern reaction was performed in the existence of bare polymer (PC4RA) and modified polymer (PC4RA@SiPrCl), functionalized polymer.

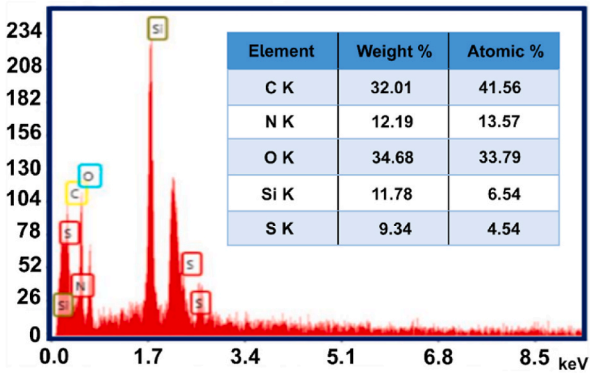

Fig. 2. Recorded EDAX pattern of PC4RA@SiPr-Pip-BuSO$_3$H catalyst.

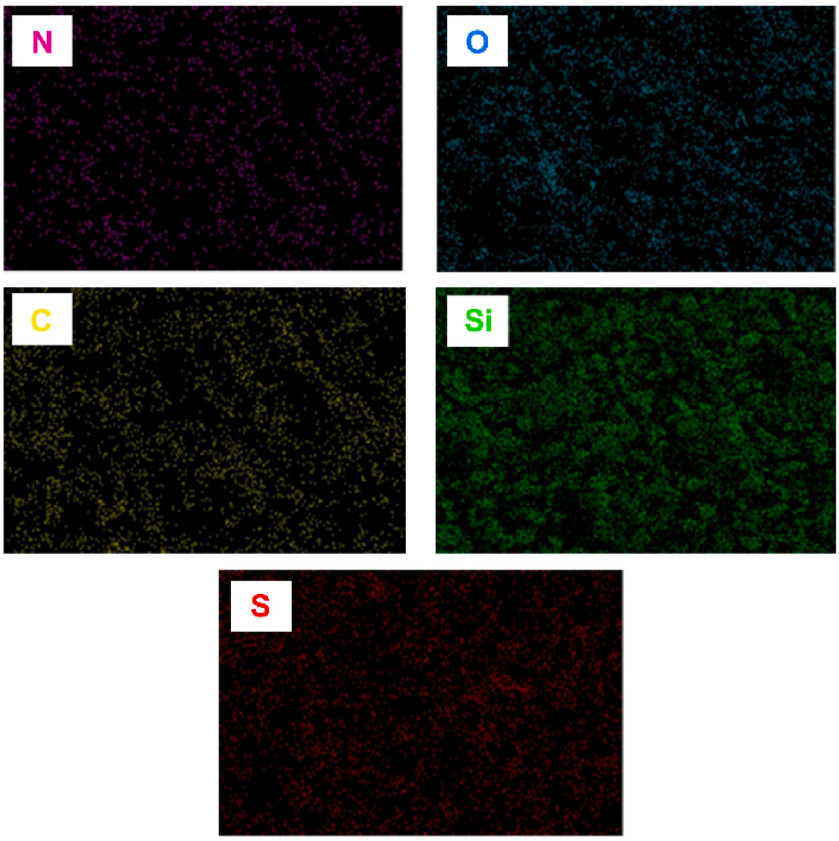

Fig. 3. Recorded elemental mapping image of PC4RA@SiPr-Pip-BuSO_3H catalyst.

(PC4RA@SiPr-Pip) that were resulted in lower yield compared with PC4RA@SiPr-Pip-BuSO_3H, verifying SO_3H behave as active moieties (Table 1, entries 16–18). Also, the homogeneous phase was studied using Pip-BuSO_3H moieties to reveal how the catalyst affected the progress of the reaction. The yield of the related product was only 63%, which showed that SO_3H was the active center. Notably, the base portion (Piperazine) and cavity-containing polymeric support (PC4RA) have a synergistic effect, enhancing the reactivity of the polymeric catalyst (Table 1, entry 19). Owing to encouraging results, PC4RA@SiPr-Pip-BuSO_3H was applied to catalyze more heterocycles from the spiro family (Table 2 and Scheme 3).

The proposed mechanism (Scheme 4) has illustrated different steps of spiro-acenaphthylene synthesis using PC4RA@SiPr-Pip-BuSO_3H. The initial interaction between acenaphthoquinone and malononitrile produces intermediate I. The nucleophilic attack on intermediate I, through the Michael addition, leads to the formation of intermediate II. Finally, the intramolecular cyclization reaction (III) results in the target product (IV). Notably, SO_3H groups act as the active site with the most contribution to the activation of compounds. Piperazine contains two tertiary amines, acting as Brønsted base, and has a synergistic effect on the reaction rate. So, Pip contributes to reaction progress (through deprotonation of compounds) but less than the acidic active site.

In the last investigation, a comparison was executed between the current work and some earlier issued catalysts to assess their efficiency (Table 3). The comparison was based on factors including the amount of catalyst loading, reaction time, temperature, and recovery times. While respecting the previous works, the present work has advantages over the former studies, especially in the number of catalyst recoveries and the amount of used catalyst (entries 1–8). In conclusion, the prepared polymeric catalyst is comparable to all previous catalysts and sometimes even superior to them. The high recycling numbers demonstrate effortless workup, high durability of the bifunctional catalyst, and the least leaching of the active sites of SO_3H. As deduced, the synergistic incorporation of Brønsted base centers (Pip) and the host-guest attribute of the cavity-containing network with active moving arms (SO_3H as a Brønsted acid) have made the high efficiency and short-time reaction. Furthermore, the presence of moving arms (Brønsted SO_3H) improves the reactivity and selectivity of the polymeric catalyst and reaction rate, which is similar to a homogeneous catalyst. As concluded from this comparison, this modified polymer with dual acidic-basic functional groups is a promising heterogeneous catalyst to use in organic reactions other than spiro derivatives.

3.2. Recovery

The dual acid-base catalyst, PC4RA@SiPr-Pip-BuSO_3H, delivered an excellent reusability, as confirmed by multiple consecutive runs (Fig. 9). After the first run, the functionalized polymer was easily filtered from the crude mixture and washed with EtOH/H_2O. It

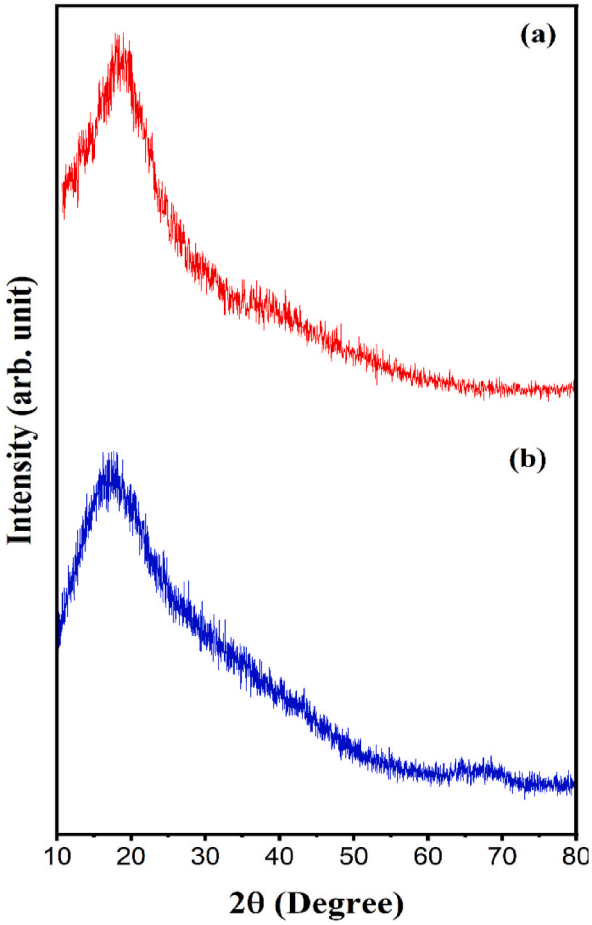

Fig. 4. XRD analysis of fresh PC4RA@SiPr-Pip-BuSO$_3$H (a) and recovered PC4RA@SiPr-Pip-BuSO$_3$H

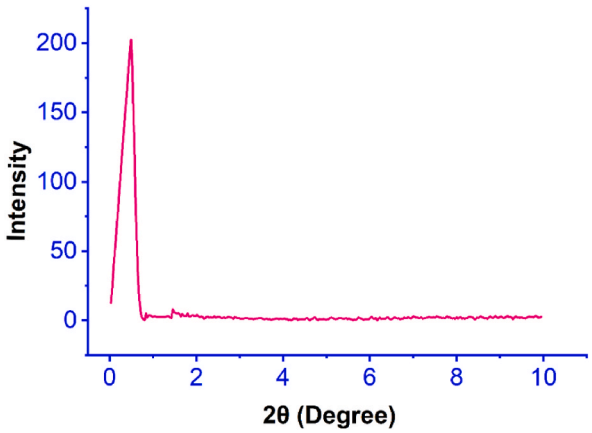

Fig. 5. LPXRD analysis of PC4RA@SiPr-Pip-BuSO$_3$H catalyst.

was then dried for 10 h using an oven at 80 °C and ready to be used again. In this stage, considering the same ratio of starting materials and the polymeric catalyst as the first run, the recovered catalyst was reused in the model reaction (10 times) under the same initial conditions. Mesoporous PC4RA@SiPr-Pip-BuSO$_3$H catalyst in nearly all consecutive recovery runs had a high yield (91–98%) and short time (10–25 min) for the corresponding product and a simple recovery method. These results revealed that the bi-functional Brønsted acidic-basic catalyst containing cavity, PC4RA@SiPr-Pip-BuSO$_3$H, has a high stability with no leaching of active sites due to the covalent bonding of functional groups. FT-IR, XRD, TEM, EDAX, and Elemental mapping analyses were used to show the

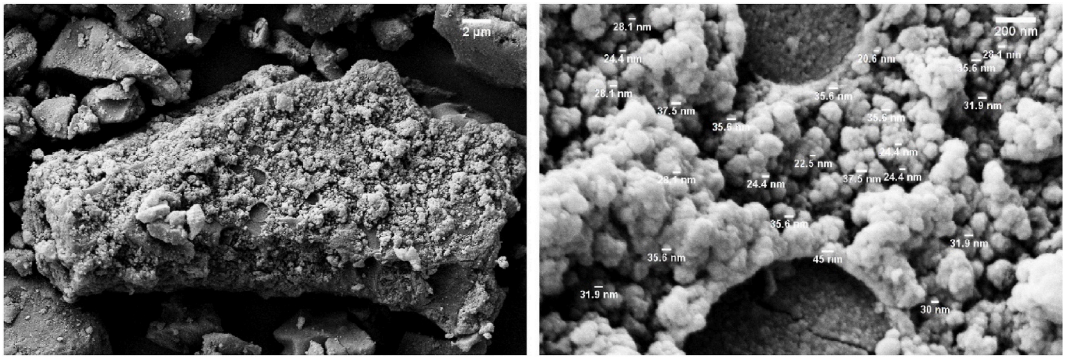

Fig. 6. Recorded SEM images of synthesized PC4RA@SiPr-Pip-BuSO_3H

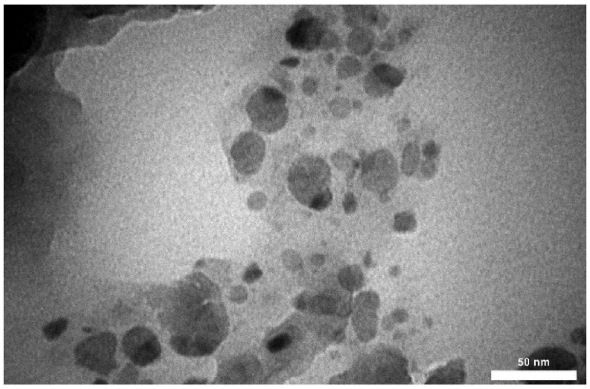

Fig. 7. Recorded TEM image of PC4RA@SiPr-Pip-BuSO_3H catalyst.

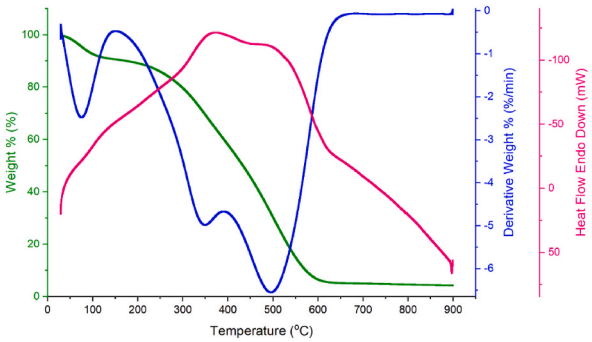

Fig. 8. The TGA diagram of PC4RA@SiPr-Pip-BuSO_3H catalyst.

chemical stability of the catalyst during the ten-run recovery.

3.2.1. Characterization of recovered catalyst

The FT-IR analysis of the recovered catalyst showed that the characteristic peaks related to the stretching vibrations of OH, S═O, Si–O, and the bending vibration of N–H at 3280–3550, 1128, 1107, and 895, 1420 cm^{-1}, respectively, were still present in the recovered structure.

These observations demonstrated that the different components of the catalyst were covalently connected and remained intact even after ten runs of recovery. No changes were observed in the recovered spectrum compared to the fresh ones, indicating the high durability of the catalyst under the applied conditions, as shown in Fig. 10.

The XRD technique was employed to demonstrate the structural stability of the reused catalyst. After 10-time recycling, the XRD analysis revealed a broad signal at around $2\theta = 16–23^{o}$, identical to the XRD pattern of the fresh ones. This result confirmed that the functionalized polymer maintained its amorphous nature throughout the recovery process and possessed a durable scaffold, as shown

Table 1
Investigation of different reaction conditions for the preparation of spiro-acenaphthylene heterocycles in the presence of PC4RA@SiPr-Pip-BuSO$_3$H as an acidic catalyst[a].

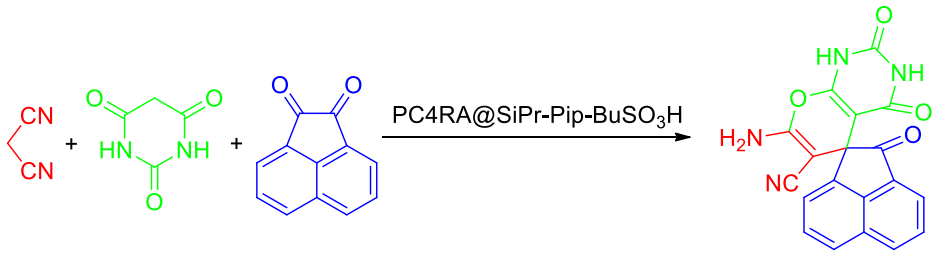

Entry	Catalyst (g)	Solvent	T (°C)	Time (min)	Yield[b] (%)
1	0.009	–	50	60	15
2	0.009	Toluene	50	60	–
3	0.009	CH_2Cl_2	50	60	–
4	0.009	MeOH	50	60	35
5	0.009	ETOH	50	60	48
6	0.009	ETOH/H_2O	50	60	66
7[c]	**0.009**	**H_2O**	**50**	**10**	**98**
8	0.007	H_2O	50	10	78
9	0.005	H_2O	50	10	69
10	–	H_2O	50	45	Trace
11	0.012	H_2O	50	10	96
12	0.009	H_2O	r.t	35	31
13	0.009	H_2O	65	25	95
14	0.009	H_2O	75	25	90
15	0.009	H_2O	95	35	90
16	PC4RA (0.009 g)	H_2O	50	10	21
17	PC4RA@SiPrCl (0.009 g)	H_2O	50	10	Trace
18	PC4RA@SiPr-Pip (0.009 g)	H_2O	50	10	72
19	Pip-BuSO$_3$H (0.009 g)	H_2O	50	10	63

[a] Conditions: malononitrile, acenaphthoquinone, and barbituric acid (1 mmol), reflux in organic solvents.
[b] Isolated yields.
[c] Optimal conditions.

in Fig. 4b.

To show possible changes in the distribution of catalyst elements and confirm their successful stabilization on the polymer surface after reusing, EDS (energy-dispersive spectroscopy) analysis and Elemental mapping were conducted (Figs. 11 and 12).

The investigation of elemental mapping outcomes showed that the expected elements of the catalyst (C, Si, N, S, and O) were uniformly distributed throughout the catalyst structure with an approximately close ratio compared to the fresh ones. This observation approved elemental composition. The same pattern as the fresh ones in EDS and Elemental mapping deeply affirms the findings of the recovered FT-IR in Fig. 10.

As concluded, based on the image provided in Fig. 13, the amorphous polymer has an outstanding ability in the permanence of acidic-basic moieties on its surface. Also, the TEM image confirms that the polymer has high power in recoverability under optimal conditions during several sequential reactions. This pattern is the same as the fresh parents, highlighting the reliability and consistency of the polymer.

3.3. Experimental procedure for heterogeneity determination (split test)

We arranged an experiment without starting materials (malononitrile, acenaphthoquinone, and barbituric acid) to demonstrate whether the catalyst acts heterogeneously or not. Initially, 0.009 g of PC4RA@SiPr-Pip-BuSO$_3$H was added to a flask containing 10 mL of water under constant stirring at 50 °C. After 10 min (optimal time), the coffee-colored catalyst was removed from the reaction media. Next, the reactants (1 mmol of malononitrile, acenaphthoquinone, and barbituric acid) were added to the remaining solution and stirred at 50 °C. As observed, no progress was observed in the reaction even after a long time (about 2 h). On the other hand, by adding the catalyst separated in the first step to the reaction mixture under optimal conditions after 10 min, the reaction proceeded with a yield of 98%. These results indicated that the PC4RA@SiPr-Pip-BuSO$_3$H catalyst acts heterogeneously.

3.4. Determination of catalyst acidity

An aqueous solution of NaCl (25 mL, 1 M) was initially regulated up to pH = 6.5, and then, 0.05 g of the designed catalyst was added to the prepared solution and stirred at room temperature for 24 h. After that, the pH was investigated and found to be 2.1,

Table 2
One-pot preparation of spiro-acenaphthylene and -oxindole derivatives in the presence of PC4RA@SiPr-Pip-BuSO$_3$H[a,b] [a] Optimized conditions: H_2O, catalyst (0.009 g), T = 50, °C, substrates (1 mmol). [b] Melting points [109–115].

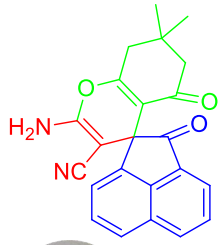


5a) Mp: 265–267 °C, 94%, 20 min

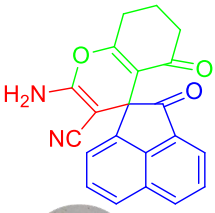


5b) Mp: 243-246 °C, 92%, 15 min

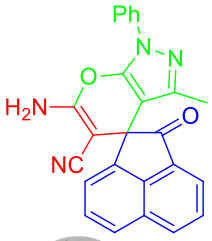


5c) Mp: 194-197 °C, 89%, 20 min

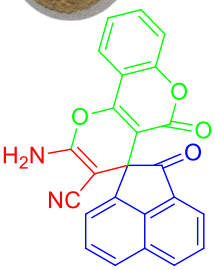


5d) Mp: 294-296 °C, 94%, 15 min

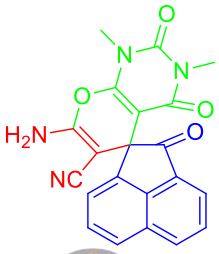


5e) Mp: 204-207 °C, 93%, 17 min

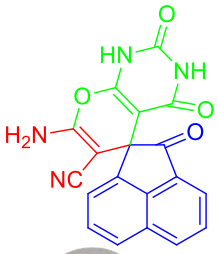


5f) Mp >300 °C, 98%, 10 min

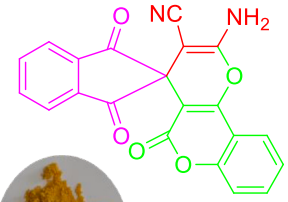


6g) Mp >300 °C, 96%, 12 min

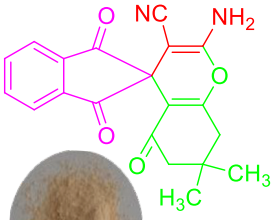


6h) Mp >300 °C, 96%, 15 min

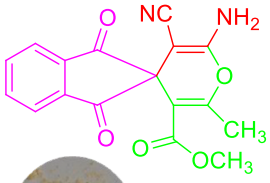


6i) Mp: 239-242 °C, 89%, 25 min

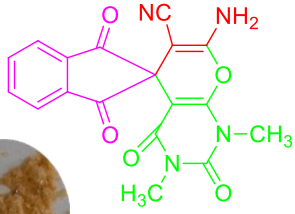


6j) Mp >300 °C, 93%, 17 min

indicating that SO_3H protons and sodium ions had undergone the ion exchange. The value of 2.1 is the SO_3H (H^+) loading on the polymer surface, calculated to be approximately 1.9 mmol g^{-1}. This consequence was further confirmed using a back-titration, which showed a similar result.

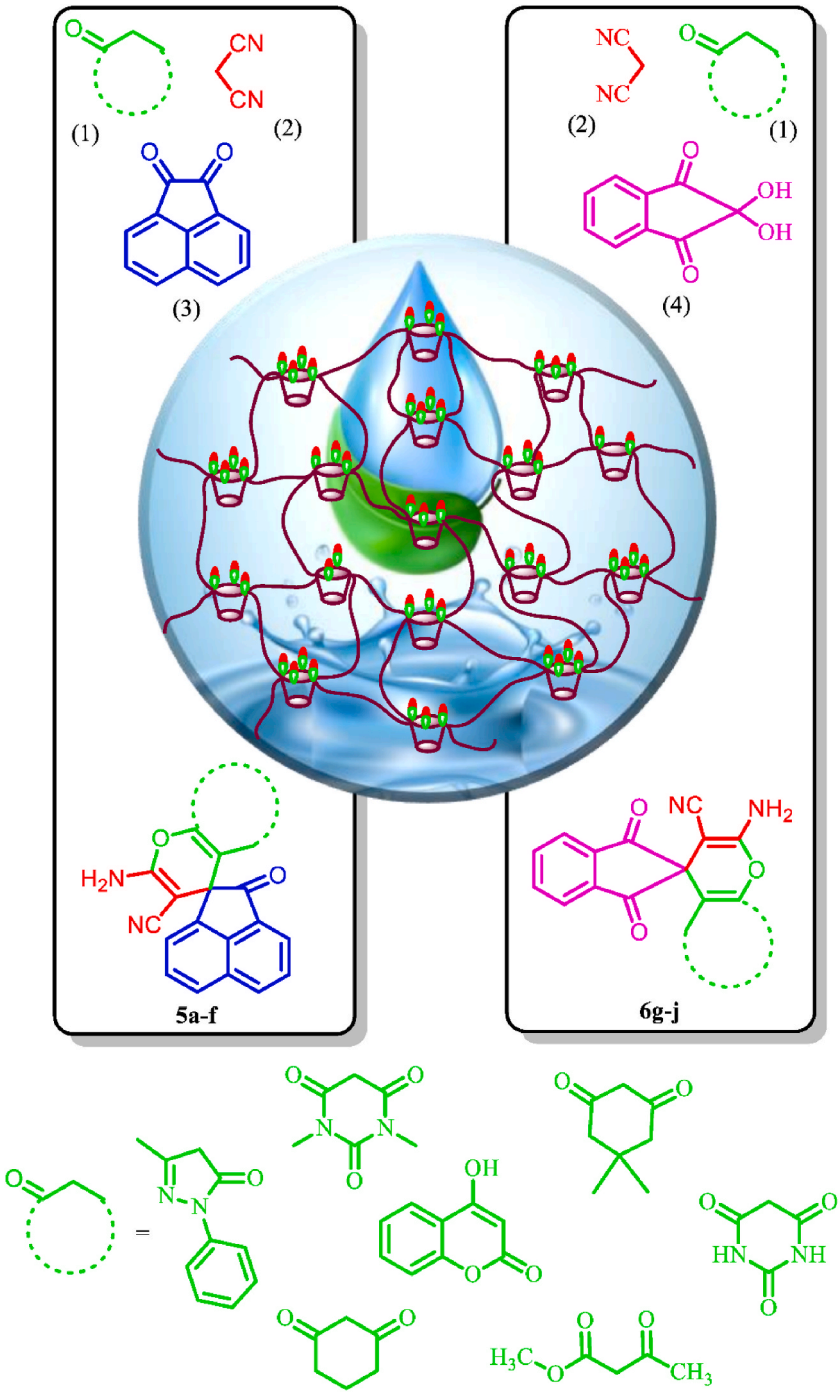

Scheme 3. Schematic presentation of the synthesis of the spiro-acenaphthylene and amino-spiro indene. Conditions: equal molar ratio of substrates (1 mmol) in aqueous media, 50 °C, and 0.009 g of PC4RA@SiPr-Pip-BuSO_3H

4. Conclusion

Polymer-supported Brønsted acidic-basic catalyst, PC4RA@SiPr-Pip-Buactive, was briefly synthesized by immobilizing piperazine and n-butyl sulfonic acid on the lower edge of 3D amorphous polycalix [4]resorcinarene and then efficiently used as a functionalized polymer for the preparation of the spiro-acenaphthylene and amino-spiroindene heterocycles. The FT-IR, EDX, and TGA techniques approved covalent stabilization of the organic-inorganic hybrid on the surface of the polycalix. The XRD, TEM, and FE-SEM analyses showed the amorphous morphology, particle size, and the presence of piperazine and *n*-butyl sulfonic acid on the polymeric support.

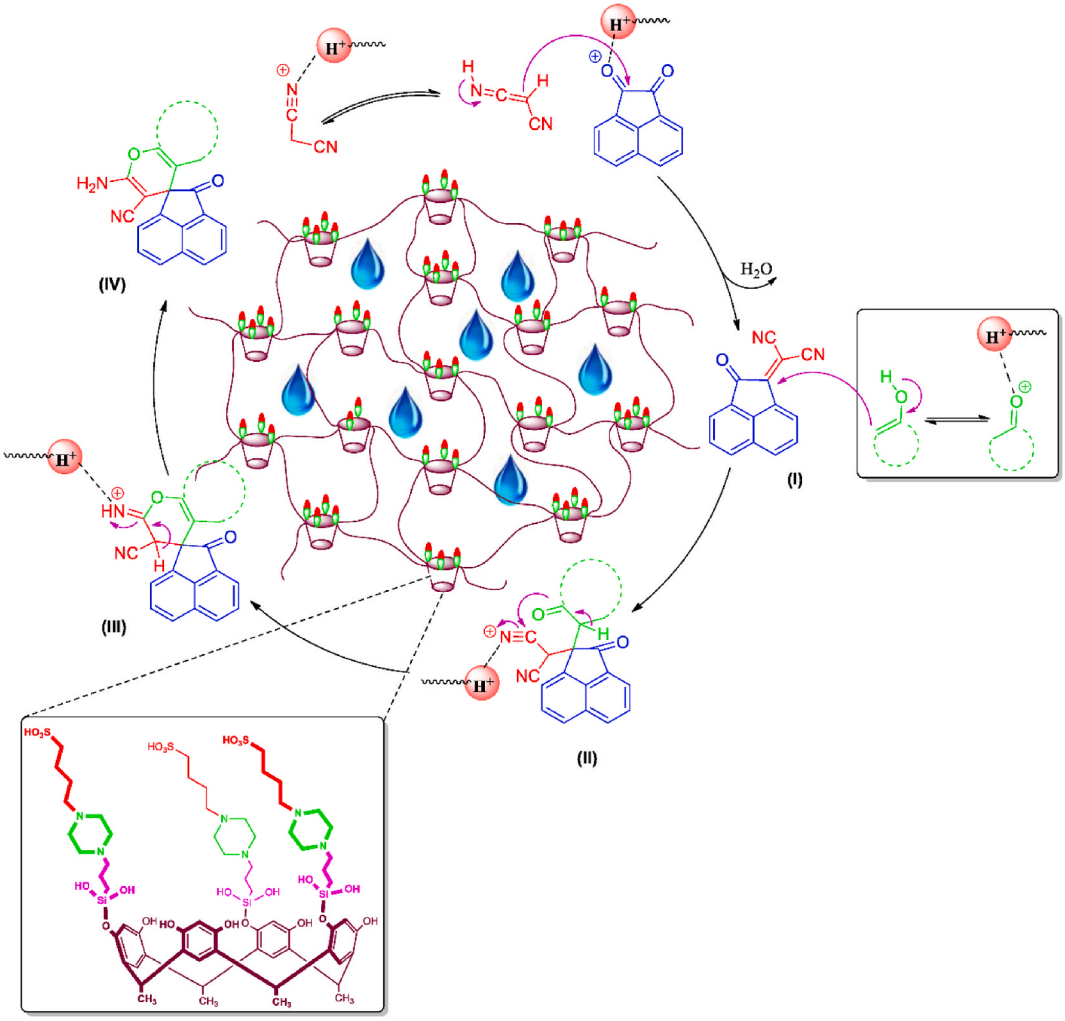

Scheme 4. Proposed mechanism for the preparation of spiro-acenaphthylene in the presence of the PC4RA@SiPr-Pip-BuSO$_3$H

Table 3
Review and comparison of the different catalysts presented in previous reports with PC4RA@SiPr-Pip-BuSO$_3$H in the synthesis of spiro-acenaphthylene heterocycles[a].

Entry	Catalyst	Conditions	Recovery times	Yield (%)	Ref
1	[HAuCl$_4$.H$_2$O]	Cat. 5 mol%, 30 min, 70 °C	–	96	[116]
2	[Et$_3$N]	Cat. 0.1 g, 10 min, 100 °C	–	85	[113]
3	[PCAgNPs]	Cat. 0.025 mmol, 20 min, reflux	4	94	[92]
4	[Fe$_2$O$_3$]	Cat. 20 mmol, 5 h, 90 °C	–	79	[117]
5	[DBU]	Cat. 10 mol%, 5 min, reflux	–	90	[118]
6	[Na$_2$eosin Y]	Cat. 1.5 mol%, 4 h, rt	–	93	[119]
7	[NiFe$_2$@SiO$_2$@Melamine]	Cat. 0.025 g, 15 min, reflux	6	94	[120]
8	[Na$_2$EDTA]	Cat. 5 mol%, 10 min, 80 °C	5	95	[112]
9	[PC4RA@SiPr-Pip-BuSO$_3$H (This wok)]	Cat. 0.009 g, 15 min, 50 °C	10	98	–

[a] PC: Preyssler functionalized cellulose, DBU: 1,8-diazabicyclo[5.4.0]undec-7-ene, EDTA: Ethylenediaminetetraacetic acid.

The LPXRD technique was applied to show the mesoporous structure. The catalytic efficiency was assessed by the spiro formation under optimal conditions, i.e., 50 °C, 0.009 g catalyst loading, and H$_2$O. The PC4RA@SiPr-Pip-BuSO$_3$H could successfully catalyze the regarded products with a high yield (89–98%). The results obtained from the synthesis of spiro-acenaphthylene and amino-spiroindene derivatives were confirmed using ^{1}HNMR, ^{13}CNMR, and FT-IR. High catalyst recoverability (10 times) was confirmed using FT-IR, EDX, elemental mapping, TEM, and PXRD analysis. The recovery results exhibited an identical mode to the parent/new catalyst, verifying remarkable durability. Facil filtration from the reaction mixture, synergistic contribution between the cavity (the guest-host

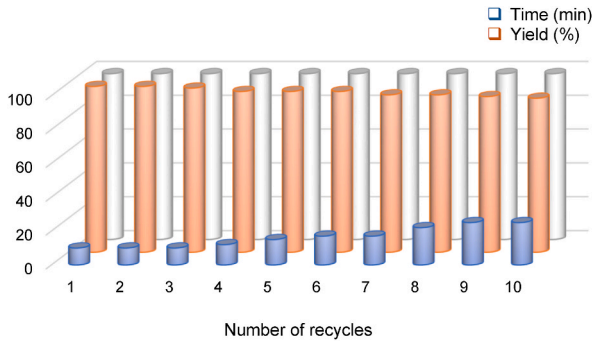

Fig. 9. Reusability of the designed catalyst during 10 runs of successive recycling.

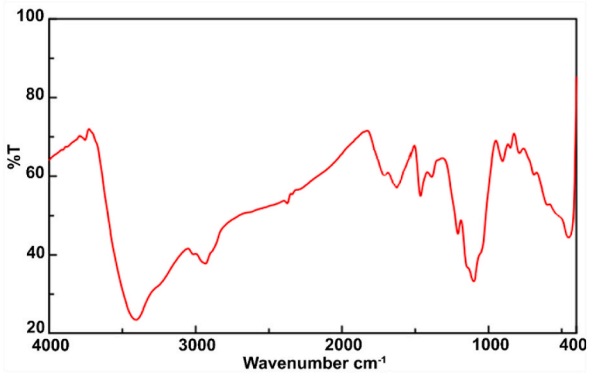

Fig. 10. FT-IR spectrum of the recycled PC4RA@SiPr-Pip-BuSO_3H

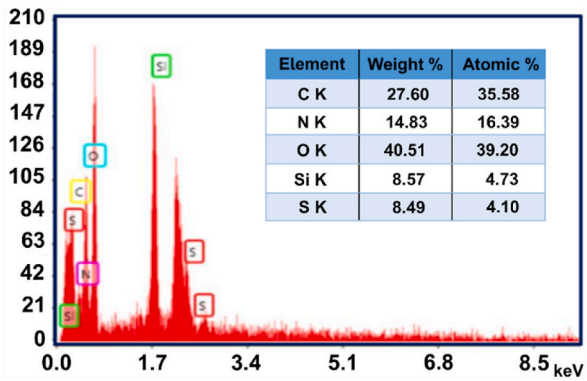

Fig. 11. Recorded EDAX pattern of the recovered PC4RA@SiPr-Pip-BuSO_3H

role) and active pendant sites, minimal leaching in active centers over the reaction, and low amount of catalyst in the reactions are other advantages of this work.

CRediT authorship contribution statement

Aref Mahmoudi Asl: Writing – original draft. **Bahador Karami:** Supervision. **Mahnaz Farahi:** Conceptualization. **Zahra Karimi:** Writing – review & editing.

Declaration of competing interest

The authors declare that they have no known competing financial interests or personal relationships that could have appeared to

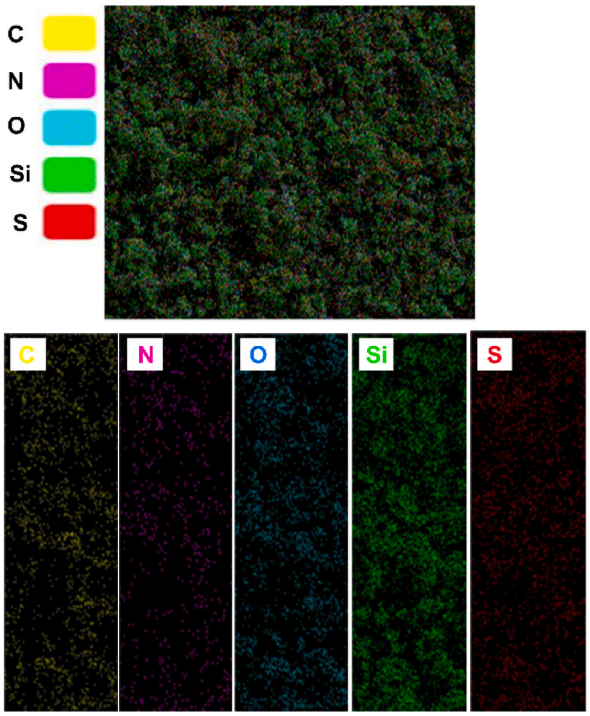

Fig. 12. Recorded elemental mapping of recovered PC4RA@SiPr-Pip-BuSO$_3$H

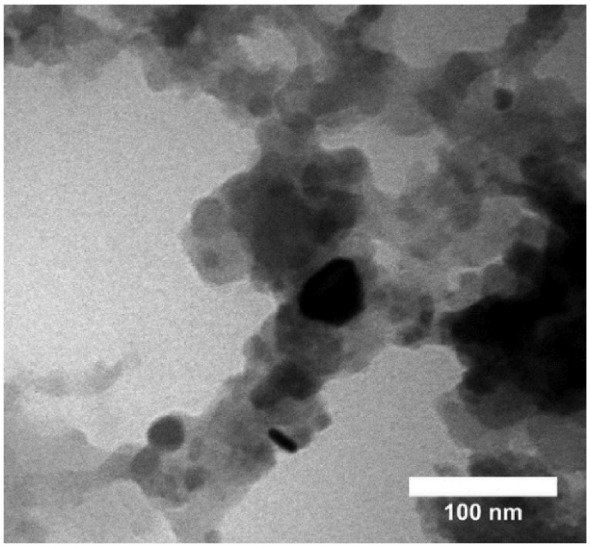

Fig. 13. TEM image of recovered PC4RA@SiPr-Pip-BuSO$_3$H catalyst.

influence the work reported in this paper.

Acknowledgements

The authors gratefully acknowledge the support for this work by Yasouj University, Iran.

Appendix A. Supplementary data

Supplementary data to this article can be found online at https://doi.org/10.1016/j.heliyon.2024.e29277.

References

[1] X. Wang, L. Xie, K. Lin, W. Ma, T. Zhao, X. Ji, M. Alyami, N.M. Khashab, H. Wang, J.L. Sessler, Calix [4] pyrrole-crosslinked porous polymeric networks for the removal of micropollutants from water, Angew. Chem., Int. Ed. 60 (2021) 7188–7196.
[2] S. Che, L. Fang, Porous ladder polymer networks, Chem 6 (2020) 2558–2590.
[3] D.-H. Yang, Y. Tao, X. Ding, B.-H. Han, Porous organic polymers for electrocatalysis, Chem. Soc. Rev. 51 (2022) 761–791.
[4] Y. Zhang, S.N. Riduan, Functional porous organic polymers for heterogeneous catalysis, Chem. Soc. Rev. 41 (2012) 2083–2094.
[5] T.-X. Wang, H.-P. Liang, D.A. Anito, X. Ding, B.-H. Han, Emerging applications of porous organic polymers in visible-light photocatalysis, J. Mater. Chem. A 8 (2020) 7003–7034.
[6] T. Zhang, G. Xing, W. Chen, L. Chen, Porous organic polymers: a promising platform for efficient photocatalysis, Mater. Chem. Front. 4 (2020) 332–353.
[7] J. Zhang, X. Yan, X. Hu, R. Feng, M. Zhou, Direct carbonization of Zn/Co zeolitic imidazolate frameworks for efficient adsorption of Rhodamine B, Chem. Eng. J. 347 (2018) 640–647.
[8] K.S. Song, P.W. Fritz, A. Coskun, Porous organic polymers for CO_2 capture, separation and conversion, Chem. Soc. Rev. 51 (2022) 9831–9852.
[9] F. Vilela, K. Zhang, M. Antonietti, Conjugated porous polymers for energy applications, Energy Environ. Sci. 5 (2012) 7819–7832.
[10] M. Kathiresan, Metal-ion/metal nanoparticle-anchored porous organic polymers as efficient catalysts for organic transformations–A recent overview, Chem. Asian J. 18 (2023) e202201299.
[11] L. Tian, S. Zhou, J. Zhao, Q. Xu, N. Li, D. Chen, H. Li, J. He, J. Lu, Sulfonate-modified calixarene-based porous organic polymers for electrostatic enhancement and efficient rapid removal of cationic dyes in water, J. Hazard Mater. 441 (2023) 129873.
[12] D. Luo, T. Shi, Q.H. Li, Q. Xu, M. Strømme, Q.F. Zhang, C. Xu, Green, general and low-cost synthesis of porous organic polymers in sub-kilogram scale for catalysis and CO_2 capture, Angew. Chem., Int. Ed. 62 (2023) e202305225.
[13] S.-Y. Ding, J. Gao, Q. Wang, Y. Zhang, W.-G. Song, C.-Y. Su, W. Wang, Construction of covalent organic framework for catalysis: Pd/COF-LZU1 in Suzuki–Miyaura coupling reaction, J. Am. Chem. Soc. 133 (2011) 19816–19822.
[14] B. Yang, H. Wang, D.W. Zhang, Z.T. Li, Water-Soluble three-dimensional polymers: non-covalent and covalent synthesis and functions, Chin. J. Chem. 38 (2020) 970–980.
[15] U. Díaz, A. Corma, Ordered covalent organic frameworks, COFs and PAFs. From preparation to application, Coord. Chem. Rev. 311 (2016) 85–124.
[16] W. Ji, T.-X. Wang, X. Ding, S. Lei, B.-H. Han, Porphyrin-and phthalocyanine-based porous organic polymers: from synthesis to application, Coord. Chem. Rev. 439 (2021) 213875.
[17] J.-S.M. Lee, A.I. Cooper, Advances in conjugated microporous polymers, Chem. Rev. 120 (2020) 2171–2214.
[18] T. Ben, S. Qiu, Porous aromatic frameworks: synthesis, structure and functions, CrystEngComm 15 (2013) 17–26.
[19] Y. Xu, S. Jin, H. Xu, A. Nagai, D. Jiang, Conjugated microporous polymers: design, synthesis and application, Chem. Soc. Rev. 42 (2013) 8012–8031.
[20] D. Zhang, H. Wang, Z. Li, Water-soluble regular three-dimensional supramolecular and covalent organic polymers, Chem. Res. Chinese Universities 41 (2020) 1139–1150.
[21] A.P. Cote, A.I. Benin, N.W. Ockwig, M. O'Keeffe, A.J. Matzger, O.M. Yaghi, Porous, crystalline, covalent organic frameworks, Science 310 (2005) 1166–1170.
[22] X. Song, W. Zhu, Y. Yan, H. Gao, W. Gao, W. Zhang, M. Jia, Triphenylamine-based porous organic polymers: synthesis and application for supporting phosphomolybdate to fabricate efficient olefin oxidation catalysts, Microporous Mesoporous Mater. 242 (2017) 9–17.
[23] J.-Y. Lee, C.D. Wood, D. Bradshaw, M.J. Rosseinsky, A.I. Cooper, Hydrogen adsorption in microporous hypercrosslinked polymers, Chem. Commun. (2006) 2670–2672.
[24] M. Tsyurupa, V. Davankov, Porous structure of hypercrosslinked polystyrene: state-of-the-art mini-review, React. Funct. Polym. 66 (2006) 768–779.
[25] S. Das, P. Heasman, T. Ben, S. Qiu, Porous organic materials: strategic design and structure–function correlation, Chem. Rev. 117 (2017) 1515–1563.
[26] S.-Y. Ding, W. Wang, Covalent organic frameworks (COFs): from design to applications, Chem. Soc. Rev. 42 (2013) 548–568.
[27] C.M. Parlett, K. Wilson, A.F. Lee, Hierarchical porous materials: catalytic applications, Chem. Soc. Rev. 42 (2013) 3876–3893.
[28] Q. Sun, Z. Dai, X. Meng, F.-S. Xiao, Porous polymer catalysts with hierarchical structures, Chem. Soc. Rev. 44 (2015) 6018–6034.
[29] A. Mouradzadegun, M.R. Ganjali, M.A. Mostafavi, Design and synthesis of a magnetic hierarchical porous organic polymer: a new platform in heterogeneous phase-transfer catalysis, Appl. Organomet. Chem. 32 (2018) e4214.
[30] J.-X. Jiang, F. Su, A. Trewin, C.D. Wood, H. Niu, J.T. Jones, Y.Z. Khimyak, A.I. Cooper, Synthetic control of the pore dimension and surface area in conjugated microporous polymer and copolymer networks, J. Am. Chem. Soc. 130 (2008) 7710–7720.
[31] P.M. Budd, E.S. Elabas, B.S. Ghanem, S. Makhseed, N.B. McKeown, K.J. Msayib, C.E. Tattershall, D. Wang, Solution-processed, organophilic membrane derived from a polymer of intrinsic microporosity, Adv. Mater. 16 (2004) 456–459.
[32] R. Chen, J.L. Shi, Y. Ma, G. Lin, X. Lang, C. Wang, Designed synthesis of a 2D porphyrin-based sp^2 carbon-conjugated covalent organic framework for heterogeneous photocatalysis, Angew. Chem., Int. Ed. 58 (2019) 6430–6434.
[33] C. Sarkar, S.C. Shit, N. Das, J. Mondal, Presenting porous–organic–polymers as next-generation invigorating materials for nanoreactors, Chem. Commun. 57 (2021) 8550–8567.
[34] P. Kaur, J.T. Hupp, S.T. Nguyen, Porous organic polymers in catalysis: opportunities and challenges, ACS Catal. 1 (2011) 819–835.
[35] J. Rahimi, M. Naderi, M. Ijdani, M. Heidari, M. Azizi, A. Maleki, Magnetite Pd-loaded nitrogen-rich porous organic polymer as a catalyst for suzuki-miyaura coupling reaction, Mater. Today Chem. 28 (2023) 101375.
[36] D.W. Kang, M. Kang, C.S. Hong, Post-synthetic modification of porous materials: superprotonic conductivities and membrane applications in fuel cells, J. Mater. Chem. A 8 (2020) 7474–7494.
[37] J.H. Kim, D.W. Kang, H. Yun, M. Kang, N. Singh, J.S. Kim, C.S. Hong, Post-synthetic modifications in porous organic polymers for biomedical and related applications, Chem. Soc. Rev. 51 (2022) 43–56.
[38] A. Modak, A. Ghosh, A.R. Mankar, A. Pandey, M. Selvaraj, K.K. Pant, B. Chowdhury, A. Bhaumik, Cross-linked porous polymers as heterogeneous organocatalysts for task-specific applications in biomass transformations, CO_2 fixation, and asymmetric reactions, ACS Sustainable Chem. Eng. 9 (2021) 12431–12460.
[39] S. Rat, A. Chavez-Sanchez, M. Jerigová, D. Cruz, M. Antonietti, Acetic anhydride polymerization as a pathway to functional porous organic polymers and their application in acid–Base catalysis, ACS Appl. Polym. Mater. 3 (2021) 2588–2597.
[40] Q. Wu, W. Gong, G. Li, Porous organic polymers with Thiourea linkages (POP-TUs): effective and recyclable Organocatalysts for the Michael reaction, ACS Appl. Mater. Interfaces 12 (2020) 17861–17869.
[41] P. Kaur, J. Hupp, S. Nguyen, Porous organic polymers in catalysis: opportunities and challenges, ACS Catal. 1 (2011) 819–835.
[42] A. Arduini, G. Manfredi, A. Pochini, A.R. Sicuri, R. Ungaro, Selective formylation of calix [4] arenes at the 'upper rim'and synthesis of new cavitands, J. Chem. Soc., Chem. Commun. (1991) 936–937.
[43] E. Akceylan, M. Yilmaz, Synthesis of calix [4] arene alkylamine derivatives as new phase-transfer catalysts for esterification reaction, Tetrahedron 67 (2011) 6240–6245.
[44] O. Sénèque, M. Giorgi, O. Reinaud, Bio-inspired calix [6] Arene–zinc funnel complexes, Supramol. Chem. 15 (2003) 573–580.
[45] E. Ozyilmaz, S. Sayin, Preparation of new calix [4] arene-immobilized biopolymers for enhancing catalytic properties of candida rugosa lipase by sol–gel encapsulation, Appl. Biochem. Biotechnol. 170 (2013) 1871–1884.
[46] H. Li, H. Huang, X. Yan, C. Liu, L. Li, A calix [4] arene-crosslinked polymer for rapid adsorption of cationic dyes in water, Mater. Chem. Phys. 263 (2021) 124295.
[47] A. Gorbunov, N. Ozerov, M. Malakhova, A. Eshtukov, D. Cheshkov, S. Bezzubov, V. Kovalev, I. Vatsouro, Assembling triazolated calix [4] semitubes by means of copper (I)-catalyzed azide–alkyne cycloaddition, Org. Chem. Front. 8 (2021) 3853–3866.
[48] Z. Lai, T. Zhao, J.L. Sessler, Q. He, Bis–calix [4] pyrroles: preparation, structure, complexation properties and beyond, Coord. Chem. Rev. 425 (2020) 213528.

[49] A. Ovsyannikov, S. Solovieva, I. Antipin, S. Ferlay, Coordination Polymers based on calixarene derivatives: structures and properties, Coord. Chem. Rev. 352 (2017) 151–186.
[50] Z. Zhang, L. Li, D. An, H. Li, X. Zhang, Triazine-based covalent organic polycalix [4] arenes for highly efficient and reversible iodine capture in water, J. Mater. Sci. 55 (2020) 1854–1864.
[51] D. Shetty, S. Boutros, A. Eskhan, A.M. De Lena, T. Skorjanc, Z. Asfari, H. Traboulsi, J. Mazher, J. Raya, F. Banat, Thioether-crown-rich calix [4] arene porous polymer for highly efficient removal of mercury from water, ACS Appl. Mater. Interfaces 11 (2019) 12898–12903.
[52] S. Abubakar, T. Skorjanc, D. Shetty, A. Trabolsi, Porous polycalix [n] arenes as environmental pollutant removers, ACS Appl. Mater. Interfaces 13 (2021) 14802–14815.
[53] M.M. Naseer, M. Ahmed, S. Hameed, Functionalized calix [4] arenes as potential therapeutic agents, Chem. Biol. Drug Des. 89 (2017) 243–256.
[54] J. Kulesza, M. Guzinski, V. Hubscher-Bruder, F. Arnaud-Neu, M. Bocheńska, Lower rim substituted p-tert-butyl-calix [4] arene. Part 16. Synthesis of 25, 26, 27, 28-tetrakis (piperidinylthiocarbonylmethylene)-p-tert-butylcalix [4] arene and its interaction with metal ions, Polyhedron 30 (2011) 98–105.
[55] M. Benounis, N. Jaffrezic, C. Martelet, I. Dumazet-Bonnamour, R. Lamartine, High sensitive surface plasmon resonance (SPR) sensor based on modified calix (4) arene self assembled monolayer for cadmium ions detection, Mater. Trans. 56 (2015) 539–544.
[56] V. Jain, P. Kanaiya, Chemistry of calix [4] resorcinarenes, Russ. Chem. Rev. 80 (2011) 75–102.
[57] J.E. Morozova, Z.R. Gilmullina, V.V. Syakaev, A.D. Voloshina, A.P. Lyubina, S.K. Amerhanova, O.B. Babaeva, V.M. Babaev, I.S. Antipin, Carboxybetaine and carboxybetaine ester derivatives of tetra (dodecyloxyphenyl)-calix [4] resorcinarene: synthesis, self-assembly and in vitro toxicity, Molbank 2023 (2023) M1562.
[58] N.E. Kashapova, R.R. Kashapov, A.Y. Ziganshina, S.K. Amerhanova, A.P. Lyubina, A.D. Voloshina, V.V. Salnikov, L.Y. Zakharova, Complexation-induced nanoarchitectonics of sulfonate cailx [4] resorcinol substituted at the upper rim by N-methyl-D-glucamine fragments: morphological transition and in vitro anticancer activity, Colloids Surf., A 643 (2022) 128796.
[59] J.E. Morozova, Z.R. Gilmullina, A.D. Voloshina, A.P. Lyubina, S.K. Amerhanova, V.V. Syakaev, O.B. Babaeva, A.Y. Ziganshina, T.A. Mukhametzyanov, A. V. Samorodov, Calix [4] resorcinarene carboxybetaines and carboxybetaine esters: synthesis, investigation of in vitro toxicity, anti-platelet effects, anticoagulant activity, and BSA binding affinities, Int. J. Mol. Sci. 23 (2022) 15298.
[60] A.M. Shumatbaeva, J.E. Morozova, Y.V. Shalaeva, A.T. Gubaidullin, A.F. Saifina, V.V. Syakaev, O.B. Bazanova, A.S. Sapunova, A.D. Voloshina, I.R. Nizameev, The novel calix [4] resorcinarene-PEG conjugate: synthesis, self-association and encapsulation properties, Colloids Surf., A 570 (2019) 182–190.
[61] R.R. Kashapov, Y.S. Razuvayeva, A.Y. Ziganshina, R.K. Mukhitova, A.S. Sapunova, A.D. Voloshina, I.R. Nizameev, M.K. Kadirov, L.Y. Zakharova, Design of N-methyl-D-glucamine-based resorcin[4]arene nanoparticles for enhanced apoptosis effects, Mol. Pharmaceutics 17 (2019) 40–49.
[62] J.E. Morozova, C.R. Myaldzina, A.D. Voloshina, A.P. Lyubina, S.K. Amerhanova, V.V. Syakaev, A.Y. Ziganshina, I.S. Antipin, Calixresorcine cavitands bearing lipophilic cationic fragments in the construction of mitochondrial-targeting supramolecular nanoparticles, Colloids Surf., A 642 (2022) 128622.
[63] G. Al'tshuler, E. Ostapova, The electrical conductivity of a network polymer based on tetraphenylcalix [4] resorcinarene, Russ. J. Phys. Chem. A 83 (2009) 1032–1035.
[64] H. Altshuler, E. Ostapova, O. Fedyaeva, L. Sapozhnikova, O. Altshuler, Novel network polymers based on calixresorcinarenes, Macromol. Symp. 181 (2002) 1–4.
[65] A. Mouradzadegun, A.R. Kiasat, P.K. Fard, 3D-network porous polymer based on calix [4] resorcinarenes as an efficient phase transfer catalyst in regioselective conversion of epoxides to azidohydrins, Catal. Commun. 29 (2012) 1–5.
[66] O. Altshuler, N. Malyshenko, G. Shkurenko, H. Altshuler, Solid-phase nanoreactor based on calix[4]resorcinarene: gel diffusion kinetics of ion exchange, Theor. Found. Chem. Eng. 43 (2009) 43–49.
[67] H. Altshuler, L. Sapozhnikova, E. Ostapova, O. Fedyaeva, O. Altshuler, Cationites based on calix[4]resorcinarene derivatives, S Solvent Extr, Ion Exch 20 (2002) 263–271.
[68] S. Shimizu, N. Shimada, Y. Sasaki, Mannich-type reactions in water using anionic water-soluble calixarenes as recoverable and reusable catalysts, Green Chem. 8 (2006) 608–614.
[69] Y.V. Shalaeva, J.E. Morozova, A. Ermakova, I. Nizameev, M. Kadirov, E.K. Kazakova, A. Konovalov, One-step synthesis of gold colloids using amidoaminocalix [4]resorcinarenes as reducing and stabilizing agents. Investigation of naproxen binding, Colloids Surf., A 527 (2017) 1–10.
[70] A.M. Ermakova, J.E. Morozova, Y.V. Shalaeva, V.V. Syakaev, I.R. Nizameev, M.K. Kadirov, I.S. Antipin, A.I. Konovalov, The supramolecular approach to the phase transfer of carboxylic calixresorcinarene-capped silver nanoparticles, Colloids Surf., A 524 (2017) 127–134.
[71] K. Kobayashi, K. Ishii, S. Sakamoto, T. Shirasaka, K. Yamaguchi, Guest-induced assembly of tetracarboxyl-cavitand and tetra (3-pyridyl)-cavitand into a heterodimeric capsule via hydrogen bonds and CH−halogen and/or CH−π interaction: control of the orientation of the encapsulated guest, J. Am. Chem. Soc. 125 (2003) 10615–10624.
[72] M. Yamanaka, M. Kawaharada, Y. Nito, H. Takaya, K. Kobayashi, Structural alteration of hybrid supramolecular capsule induced by guest encapsulation, J. Am. Chem. Soc. 133 (2011) 16650–16656.
[73] R.R. Kashapov, S.V. Kharlamov, Y.S. Razuvayeva, A.Y. Ziganshina, I.R. Nizameev, M.K. Kadirov, S.K. Latypov, L.Y. Zakharova, Supramolecular assemblies involving calix[4]resorcinol and surfactant with pH-induced morphology transition for drug encapsulation, J. Mol. Liq. 261 (2018) 218–224.
[74] R.R. Kashapov, Y.S. Razuvayeva, A.Y. Ziganshina, R.K. Mukhitova, L.Y. Zakharova, N-methyl-D-glucaminocalix[4]resorcinol and its complexes with N-hexadecyl-N'-methyl viologen: self-assembly and encapsulation activities, Colloids Surf., A 583 (2019) 124033.
[75] J.-L. Liu, M. Sun, Y.-H. Shi, X.-M. Zhou, P.-Z. Zhang, A.-Q. Jia, Q.-F. Zhang, Functional modification, self-assembly and application of calix [4] resorcinarenes, J. Inclusion Phenom, Macrocyclic Chem. 102 (2022) 201–233.
[76] S. Sobhani, M.S. Ghasemzadeh, M. Honarmand, Piperidine and piperazine immobilized on iron oxide nanoparticles as magnetically recyclable heterogeneous catalysts for one-pot synthesis of β-phosphonomalonates, Catal. Lett. 144 (2014) 1515–1523.
[77] J.K. Augustine, Y.A. Naik, A.B. Mandal, N. Chowdappa, V.B. Praveen, Gem-dibromomethylarenes: a convenient substitute for noncommercial aldehydes in the Knoevenagel− Doebner reaction for the synthesis of α, β-unsaturated carboxylic acids, J. Org. Chem. 72 (2007) 9854–9856.
[78] S. Fioravanti, L. Pellacani, P.A. Tardella, M.C. Vergari, Facile and highly stereoselective one-pot synthesis of either (E)-or (Z)-nitro alkenes, Org. Lett. 10 (2008) 1449–1451.
[79] J.-F. Zhou, One-step synthesis of pyridine and 4H-pyran derivatives from bisarylidenecyclohexanone and malononitrile under microwave irradiation, Synth. Commun. 33 (2003) 99–103.
[80] W. Xie, H. Wang, Synthesis of heterogenized polyoxometalate-based ionic liquids with Brönsted-Lewis acid sites: a magnetically recyclable catalyst for biodiesel production from low-quality oils, J. Ind. Eng. Chem. 87 (2020) 162–172.
[81] J. Davarpanah, A.R. Kiasat, Nano Brönsted solid acid containing double-charged diazoniabi-cyclo [2.2. 2] octane chloride supported on nano rice husk silica: an efficient catalyst for the one-pot synthesis of phthalazine compounds, RSC Adv. 5 (2015) 7986–7993.
[82] Q. Zhang, H. Su, J. Luo, Y. Wei, A magnetic nanoparticle supported dual acidic ionic liquid: a "quasi-homogeneous" catalyst for the one-pot synthesis of benzoxanthenes, Green Chem. 14 (2012) 201–208.
[83] R. Gupta, M. Yadav, R. Gaur, G. Arora, P. Rana, P. Yadav, A. Adholeya, R.K. Sharma, Silica-coated magnetic-nanoparticle-supported DABCO-derived acidic ionic liquid for the efficient synthesis of bioactive 3, 3-di (indolyl) indolin-2-ones, ACS Omega 4 (2019) 21529–21539.
[84] A. Wawrzyńczak, S. Jarmolińska, I. Nowak, Nanostructured KIT-6 materials functionalized with sulfonic groups for catalytic purposes, Catal. Today 397 (2022) 526–539.
[85] R.S. Kumar, A.I. Almansour, N. Arumugam, F. Mohammad, R.R. Kumar, In vitro mechanistic exploration of novel spiropyrrolidine heterocyclic hybrids as anticancer agents, Front. Chem. 8 (2020) 465.
[86] T.L. Pavlovska, R.G. Redkin, V.V. Lipson, D.V. Atamanuk, Molecular diversity of spirooxindoles. Synthesis and biological activity, Mol. Divers. 20 (2016) 299–344.

[87] G. Kumari, M. Modi, S.K. Gupta, R.K. Singh, Rhodium (II) acetate-catalyzed stereoselective synthesis, SAR and anti-HIV activity of novel oxindoles bearing cyclopropane ring, Eur. J. Med. Chem. 46 (2011) 1181–1188.
[88] K. Warburg, H. Kruse, S. Grimme, K. Hübel, D. Rauh, H. Waldmann, Identification of thiazolidinones spiro-fused to indolin-2-ones as potent and selective inhibitors of the Mycobacterium tuberculosis protein tyrosine phosphatase B, Angew. Chem., Int. Ed. 49 (2010) 1002.
[89] M.R.P. Heravi, P. Aghamohammadi, E. Vessally, Green synthesis and antibacterial, antifungal activities of 4H-pyran, tetrahydro-4H-chromenes and spiro2-oxindole derivatives by highly efficient Fe_3O_4@ SiO_2@ NH_2@ Pd $(OCOCH_3)_2$ nanocatalyst, J. Mol. Struct. 1249 (2022) 131534.
[90] B. Borah, K.D. Dwivedi, L.R. Chowhan, Review on synthesis and medicinal application of dihydropyrano [3, 2-b] pyrans and spiro-pyrano [3, 2-b] pyrans by employing the reactivity of 5-hydroxy-2-(hydroxymethyl)-4 H-pyran-4-one, Polycyclic Aromat, Compd 42 (2022) 5893–5937.
[91] S. Wang, Y. Jiang, S. Wu, G. Dong, Z. Miao, W. Zhang, C. Sheng, Meeting organocatalysis with drug discovery: asymmetric synthesis of 3, 3′-Spirooxindoles fused with tetrahydrothiopyrans as novel p53-MDM2 inhibitors, Org. Lett. 18 (2016) 1028–1031.
[92] S. Saneinezhad, L. Mohammadi, V. Zadsirjan, F.F. Bamoharram, M.M. Heravi, Silver nanoparticles-decorated Preyssler functionalized cellulose biocomposite as a novel and efficient catalyst for the synthesis of 2-amino-4 H-pyrans and spirochromenes, Sci. Rep. 10 (2020) 14540.
[93] Y.M. Litvinov, A.M. Shestopalov, Synthesis, structure, chemical reactivity, and practical significance of 2-amino-4H-pyrans, Adv. Heterocycl. Chem. 103 (2011) 175–260.
[94] D. Kumar, V.B. Reddy, S. Sharad, U. Dube, S. Kapur, A facile one-pot green synthesis and antibacterial activity of 2-amino-4H-pyrans and 2-amino-5-oxo-5, 6, 7, 8-tetrahydro-4H-chromenes, Eur. J. Med. Chem. 44 (2009) 3805–3809.
[95] A.M. Asl, B. Karami, Z. Karimi, Tungstic acid-functionalized polycalix [4] resorcinarene as a cavity-containing hyper-branched supramolecular and recoverable acidic catalyst in 4H-pyran synthesis, RSC Adv. 13 (2023) 13374–13383.
[96] M.S. Esmaeili, M.R. Khodabakhshi, A. Maleki, Z. Varzi, Green, natural and low cost xanthum gum supported Fe_3O_4 as a robust biopolymer nanocatalyst for the one-pot synthesis of 2-amino-3-cyano-4H-pyran derivatives, Polycyclic Aromat, Compd 41 (2021) 1953–1971.
[97] B. Maleki, S. Sheikh, One-pot synthesis of 2-amino-2-chromene and 2-amino-3-cyano-4H-pyran derivatives promoted by potassium fluoride, Org. Prep. Proced. Int. 47 (2015) 368–378.
[98] S.G. Azarnier, M. Esmkhani, Z. Dolatkhah, S. Javanshir, Collagen-coated superparamagnetic iron oxide nanoparticles as a sustainable catalyst for spirooxindole synthesis, Sci. Rep. 12 (2022) 6104.
[99] M. Srivastava, P. Rai, J. Singh, J. Singh, Bmim (OH)/chitosan/C_2H_5OH synergy: grinding induced, a new route for the synthesis of spiro-oxindole and its derivatives, RSC Adv. 4 (2014) 30592–30597.
[100] H. Naeimi, S. Lahouti, Sulfonated chitosan encapsulated magnetically Fe_3O_4 nanoparticles as effective and reusable catalyst for ultrasound-promoted rapid, three-component synthesis of spiro-4H-pyrans, J. Iran. Chem. Soc. 15 (2018) 2017–2031.
[101] S.F. Hojati, A. Amiri, S. Mohamadi, N. MoeiniEghbali, Novel organometallic nanomagnetic catalyst for multicomponent synthesis of spiroindoline derivatives, Res. Chem. Intermed. 44 (2018) 2275–2287.
[102] X. Song, Y.-X. Li, L. Zhou, N. Liu, Z.-Q. Wu, Controlled synthesis of one-handed helical polymers carrying achiral organoiodine pendants for enantioselective synthesis of quaternary all-carbon stereogenic centers, Macromolecules 55 (2022) 4441–4449.
[103] M. Rouhi, B. Sadeghi, M. Moslemin, Nano-cellulose-$SBCL_5$ as a new heterogeneous nano catalyst for the one-pot synthesis of spirooxindoles under mild conditions, Bulg, Chem. Commun. 50 (2018) 23–28.
[104] B. Kumar, N.J. Babu, R.L. Chowhan, Sustainable synthesis of highly diastereoselective & fluorescent active spirooxindoles catalyzed by copper oxide nanoparticle immobilized on microcrystalline cellulose, Appl. Organomet. Chem. 36 (2022) e6742.
[105] S.F. Hojati, A. Amiri, M. Mahamed, Polystyrene@ graphene oxide-Fe_3O_4 as a novel and magnetically recyclable nanocatalyst for the efficient multi-component synthesis of spiro indene derivatives, Res. Chem. Intermed. 46 (2020) 1091–1107.
[106] S. Paul, A.R. Das, Dual role of the polymer supported catalyst PEG-OSO_3H in aqueous reaction medium: synthesis of highly substituted structurally diversified coumarin and uracil fused spirooxindoles, Tetrahedron Lett. 54 (2013) 1149–1154.
[107] M. Nasseri, B. Zakerinasab, Sulfuric acid-modified poly (ethylene glycol): an efficient, biodegradable, and reusable polymeric catalyst for synthesis of spiro oxindole derivatives in aqueous medium, Res. Chem. Intermed. 41 (2015) 5261–5270.
[108] Z. Karimi, B. Karami, A.M. Asl, 3D mesoporous polycalix-functionalized dual bronsted-Lewis acidic double-charged DABCO-based ionic liquid: as a powerful and recyclable supramolecular polymeric catalyst for spiro-fused [4H-pyran] synthesis in green solvent, New J. Chem. 47 (2023) 14469–14483.
[109] T.W. Quadri, L.O. Olasunkanmi, E.D. Akpan, A. Alfantazi, I. Obot, C. Verma, A.M. Al-Mohaimeed, E.E. Ebenso, M. Quraishi, Chromeno-carbonitriles as corrosion inhibitors for mild steel in acidic solution: electrochemical, surface and computational studies, RSC Adv. 11 (2021) 2462–2475.
[110] M.N. Elinson, A.I. Ilovaisky, V.M. Merkulova, P.A. Belyakov, F. Barba, B. Batanero, General non-catalytic approach to spiroacenaphthylene heterocycles: multicomponent assembling of acenaphthenequinone, cyclic CH-acids and malononitrile, Tetrahedron 68 (2012) 5833–5837.
[111] Z. Amiri, M. Bayat, A catalyst-free approach to synthesis of spiroacenaphthylene-pyranopyrazole derivatives in water media, Mol. Divers. 25 (2021) 121–129.
[112] T. Jazinizadeh, M.T. Maghsoodlou, R. Heydari, A. Yazdani-Elah-Abadi, Na_2EDTA: an efficient, green and reusable catalyst for the synthesis of biologically important spirooxindoles, spiroacenaphthylenes and spiro-2-amino-4H-pyrans under solvent-free conditions, J. Iran. Chem. Soc. 14 (2017) 2117–2125.
[113] M. Saeedi, M.M. Heravi, Y.S. Beheshtiha, H.A. Oskooie, One-pot three-component synthesis of the spiroacenaphthylene derivatives, Tetrahedron 66 (2010) 5345–5348.
[114] Y. He, H. Guo, J. Tian, A simple three-component synthesis of spiro-pyran derivatives, J. Chem. Res. 35 (2011) 528–530.
[115] S.-S. Jin, M.-H. Ding, H.-Y. Guo, Ionic liquid catalyzed one-pot synthesis of spiropyran derivatives via three-component reaction in water, Heterocycl, Commun. Now. 19 (2013) 139–143.
[116] M. Kidwai, A. Jahan, N.K. Mishra, Gold (III) chloride ($HAuCl_4$ $3H_2O$) in PEG: a new and efficient catalytic system for the synthesis of functionalized spirochromenes, Appl. Catal., A 425 (2012) 35–43.
[117] M.T. Maghsoodlou, R. Heydari, F. Mohamadpour, M. Lashkari, Fe_2O_3 as an environmentally benign natural catalyst for one-pot and solvent-free synthesis of spiro-4H-pyran derivatives, Iranian Iran. J. Chem. Chem. Eng. 36 (2017) 31–38.
[118] P. Saluja, K. Aggarwal, J.M. Khurana, One-pot synthesis of biologically important spiro-2-amino-4H-pyrans, spiroacenaphthylenes, and spirooxindoles using DBU as a green and recyclable catalyst in aqueous medium, Synth. Commun. 43 (2013) 3239–3246.
[119] F. Mohamadpour, New role for photoexcited organic dye, Na_2eosin Y via the direct hydrogen atom transfer (HAT) process in photochemical visible-light-induced synthesis of spiroacenaphthylenes and 1H-pyrazolo [1, 2-b] phthalazine-5, 10-diones under air atmosphere, Dyes Pigm 194 (2021) 109628.
[120] N.H. Nasab, J. Safari, Synthesis of a wide range of biologically important spiropyrans and spiroacenaphthylenes, using $NiFe_2O_4$@ SiO_2@Melamine magnetic nanoparticles as an efficient, green and reusable nanocatalyst, J. Mol. Struct. 1193 (2019) 118–124.